EUROFUSION WPJET1-PR(16) 14897

M Goniche et al.

Ion Cyclotron Resonance Heating for tungsten control in various JET H-mode scenarios

Preprint of Paper to be submitted for publication in
Plasma Physics and Controlled Fusion

This work has been carried out within the framework of the EUROfusion Consortium and has received funding from the Euratom research and training programme 2014-2018 under grant agreement No 633053. The views and opinions expressed herein do not necessarily reflect those of the European Commission.

Ion Cyclotron Resonance Heating for tungsten control in various JET H-mode scenarios

M.Goniche[1], R.J.Dumont[1], V.Bobkov[2], P.Buratti[3], S.Brezinsek[4], C.Challis[5], L.Colas[1], A.Czarnecka[6], P.Drewelow[2], N.Fedorczak[1], J.Garcia[1], C.Giroud[5], M.Graham[5], J.P.Graves[7] , J.Hobirk[2], P.Jacquet[5], E.Lerche[8], P.Mantica[9], I.Monakhov[5], P.Monier-Garbet[1], M.F.F. Nave[10], C.Noble[5], I.Nunes[10], T.Pütterich[2], F.Rimini[5], M.Valisa[11] , D. Van Eester[8] and JET Contributors*

EUROfusion Consortium, JET, Culham Science Centre, Abingdon, OX14 3DB, UK

[1]*CEA, IRFM, F-13108 Saint-Paul-lez-Durance, France.*
[2]*Max-Planck-Institut für Plasmaphysik, EURATOM-Assoziation, Garching, Germany*
[3]*ENEA, C.R. Frascati, Via E. Fermi 45 00044 Frascati (RM), Italy*
[4]*Forschungszentrum Jülich GmbH, Institut für Energie- und Klimaforschung – Plasmaphysik, Partner of the Trilateral Euregio Cluster (TEC), 52425 Jülich, Germany*
[5]*CCFE, Culham Science Centre, Abingdon, OX14 3DB, UK.*
[6]*IPPLM, Hery 23, 01-497 Warsaw, Poland*
[7]*Ecole Polytechnique Fédérale de Lausanne (EPFL), Centre de Recherches en Physique des Plasmas,1015 Lausanne, Switzerland*
[8] *1LPP-ERM/KMS, EUROfusion Consortium Member - Trilateral Euregio Cluster, Brussels, Belgium*
[9]*Istituto di Fisica del Plasma 'P.Caldirola', Consiglio Nazionale delle Ricerche, Milano, Italy*
[10]*Instituto de Plasmas e Fusão Nuclear, IST, Universidade de Lisboa, Portugal*
[11]*Consorzio RFX, Consiglio Nazionale delle Ricerche, Padova, Italy*

** See the Appendix of F. Romanelli et al., Proc. of the 25th IAEA Fusion Energy Conference, 2014, St. Petersburg, Russia*

Abstract

Ion Cyclotron Resonance Heating (ICRH) in the hydrogen minority scheme provides central ion heating and acts favorably on the core tungsten transport. Full wave modeling shows that, at medium power level (4MW), after collisional redistribution, the ratio of power transferred to the ions and the electrons vary little with the minority (hydrogen) concentration n_H/n_e but the high-Z impurity screening provided by the fast ions temperature increases with the concentration.

The power radiated by tungsten in the core of the JET discharges has been analyzed on a large database covering the 2013-2014 campaign. In the baseline scenario with moderate plasma current (Ip=2.5MA) ICRH modifies efficiently tungsten transport to avoid its accumulation in the plasma centre and, when the ICRH power is increased, the tungsten

radiation peaking evolves as predicted by the neo-classical theory. At higher current (3-4MA), tungsten accumulation can be only avoided with 5MW of ICRH power with high gas injection rate. For discharges in the hybrid scenario, the strong initial peaking of the density leads to strong tungsten accumulation. When this initial density peaking is slightly reduced, with an ICRH power in excess of 4MW,very low tungsten concentration in the core (~10^{-5}) is maintained for 3 seconds. MHD activity plays a key role in tungsten transport and modulation of the tungsten radiation during a sawtooth cycle is correlated to the fishbone activity triggered by the fast ion pressure gradient.

1. Introduction

In order to prepare the ITER plasma scenarios, the divertor and first wall of the JET tokamak has been changed in 2011. The main chamber plasma facing components are made of beryllium, and the divertor is made of either plain tungsten tiles or tungsten-coated tiles (ITER-like wall, ILW). Tungsten like all high Z atoms, has a very high radiation capability which leads to a detrimental effect on plasma performance if this impurity concentration in the core is too high. It is generally admitted that the concentration has to be kept below 10^{-4} [Kallenbach 2005]. Neoclassical theory predicts an inward pinch leading to an accumulation of high Z impurities in the very core of the plasma (r/a<0.2). Moreover, strong plasma rotation occurs in neutral beam heated plasmas and the resulting centrifugal force is the cause of poloidal asymmetry enhancing the radiation on the low field side of the plasma. [Angioni 2009, Angioni 2014, Casson 2014].

This deleterious effect is mitigated by temperature screening and the sign of convection can be reversed when the ion temperature gradient is sufficiently large with respect of the ion density gradient. Under some assumptions which can be found in ref. [Angioni 2014, Casson 2014], when the poloidal asymmetries are not considered the tungsten, like all high Z impurities, flux can be expressed as

$\Gamma w \sim n_i T_i \nu_{iW} Z_W (R/L_{ni} - 0.5R/L_{Ti}) \sim n_i T_i^{-1/2} Z_W (R/L_{ni} - 0.5R/L_{Ti})$

where L_X is the inverse of the logarithmic gradient d[log(X)]/dR. However these poloidal asymmetries, arising from the centrifugal force, are important for heavy impurities and an additional term with a positive sign (inward flux) has to be added to the expression of the tungsten flux.

In addition turbulent transport can contribute to impurity transport, although for heavy impurities such as tungsten, modelling combining neoclassical and gyrokinetic codes indicates that neoclassical transport dominates on turbulent transport in the very core of the discharge [Angioni 14].

Ion cyclotron resonance heating (ICRH) can beneficially affect the tungsten transport for several reasons. Firstly, depending on the details of the minority heating scheme (mainly the minority species and concentration) and the plasma parameters (mainly the electron and ion temperatures), a large part of wave energy can be transferred to the bulk ions either by Coulomb collisions with the fast minority ions or by direct damping on the majority ions [Mantsinen 99, Dumont 13, Mantsinen 15]. Secondly, the fast ion tail, characterized by a temperature T_f, can contribute to the impurity screening [Casson 2014] as the screening scales as $n_f T_f^{-1/2}(R/L_{Tf})$ and very local deposition of ICRH leads to normalized gradient R/L_{Tf} which can exceed 5. Thirdly, the poloidal asymmetry of tungsten radiation, due to the centrifugal force in strongly rotating plasmas with NBI heating, is reduced by the temperature anisotropy of the minority species [Bilato 14]. In addition to the neo-classical effects, turbulent transport can be enhanced by core electron heating provided by ICRH waves. This effect is very likely a major player in Asdex Upgrade low-collisionality plasmas where a moderate ECRH power on top of the NBI power allows a control of the core tungsten concentration [Püterrich 13]. Finally, MHD activity and particularly core (1,1) modes with poloidal number m=1 and toroidal number n=1, can allow a flushing of the tungsten from the core of the discharge [Hender 16].

The drawback of using ICRH in metallic environment is related to enhanced high Z material sputtering arising from ions accelerated by the DC rectified potential [Jacquet 14, Bobkov 14, Czarnecka 14]. This potential can exceed 100V and light impurities, such as beryllium for the ILW case, are accelerated in the rectified sheath above the sputtering threshold of tungsten. Therefore the main issue when using ICRH is whether or not the beneficial effect on high Z impurities transport overcomes the detrimental increase of the tungsten source.

The effect of ICRH on transport of metallic impurities has been studied on JET with the carbon wall by an injection of nickel and molybdenum performed by a laser blow-off technique [Valisa 2011]. For L-mode discharges performed at rather low plasma current (I_p=1.5-2.3MA), it was found that the convection was reversed from inward to outward when

the ICRH power exceeded 3MW in the H or He^3 minority heating scheme. With the ILW, beneficial effect of ICRH power for avoiding tungsten accumulation in the plasma core has been reported at low to moderate plasma current ($I_p \leq 2.5$MA) [Goniche 14, Casson14, Giroud15, Lerche 14]. In the hybrid scenario, central ICRH heating mitigates the tungsten accumulation at least in the early time of the high power phase [Mantica 15].

In this paper, tungsten radiation from ICRH-heated plasmas is analyzed on a large database covering the JET baseline scenario with plasma current in the 2.5-4MA range (Bt=2.7-3.8T) and the hybrid scenario at 2.5MA (Bt~2.9T). ICRH power up to 6MW could be applied in these plasmas, thanks to the beneficial effect of deuterium as injection from the main chamber valves located either in the mid-plane or at the top of the vacuum vessel [Lerche 14b, Jacquet 16]. However the RF power does not exceed 20% of the total injected power, mainly provided by neutral beams injection (NBI).

Radiation and concentration of tungsten in the core of the discharge are derived from the soft X-ray (SXR) diagnostic following the inversion procedure detailed elsewhere [Pütterich 12], providing a poloidal map of these quantities as long as the electron temperature exceeds 1.5keV which is the case in the analyzed discharge at least in the inner half of the plasma ($r/a \leq 0.5$) and in most cases in even a wider volume. For the calculation of the radiated power and tungsten concentration, it is assumed that all the radiation is from tungsten. From the poloidal asymmetry of the SXR radiation, the toroidal rotation was calculated and compared to the measurements from the charge exchange spectroscopy diagnostic. A very good agreement was found for discharges performed from the beginning to the end of the 2014 campaign and we conclude that lighter metal impurities (Mo and Ni) do not contribute significantly to the SXR radiation in the plasma core ($r/a<0.5$). VUV spectroscopy also indicates that tungsten is the main high-Z impurity. As a rule of thumb a power volume density of $0.1MW/m^3$ corresponds to a tungsten concentration of 10^{-4} which is usually considered as the upper limit to maintain high performance. In the following of this paper we define the tungsten peaking factor is defined as the ratio of the flux surface-averaged radiation power densities $PF_{0.3} = P_{rad}\text{-}W(r/a=0) / P_{rad}\text{-}W(r/a=0.3)$ and $PF_{0.5} = P_{rad}\text{-}W(r/a=0) / P_{rad}\text{-}W(r/a=0.5)$.

The ion temperature in the very core of the discharge ($r/a<0.3$) is not measured for the discharges analyzed here and the following proxy will be used for the tungsten flux in

the core $\Gamma w \sim R/L_{ne} - 0.5R/L_{Te}$ that is to say $n_i=n_e$ and $T_i=T_e$, although these identities are not strictly necessary but only homothetic profiles $n_i=k_n n_e$ and $T_i=k_T T_e$ in the core region.

Section 2 presents full wave modeling of the ICRH absorption for different minority species concentration and redistribution of the power with the Coulomb collisions. The tungsten screening by the fast ion tails is estimated. The effect of the ion cyclotron resonance position on the experimental tungsten peaking and MHD activity during the sawtooth cycle are analyzed in section 3. In the two next sections, we present the experimental tungsten radiation in the plasma core on a large data base covering the whole 2013-14 JET campaign for discharges in the baseline scenario (section 4) and the hybrid scenario (section 5). These results are discussed and some conclusions drawn in the last section.

2. Modelling of the ICRH damping and temperature screening by the fast ions

In order to investigate the mechanism of ICRH power deposition when the hydrogen minority concentration n_H/n_e is varied, the EVE/AQL code [Dumont 2009, Dumont 2013] was run for a high power discharge (P_{NBI}=24MW, P_{ICRH}=4MW) with n_H/n_e varying between 0.25% and 15% while keeping the electron and bulk ion temperature profile identical ($T_e(0)$=7.5keV and $T_i(0)$=7.5 keV). When the minority concentration is increased, wave energy is transferred from the deuterium (majority 2nd harmonic heating scheme) to the hydrogen (minority 1st harmonic heating scheme) whereas the fraction damped directly on the electrons does not vary much (Figure 1-a). The fast ion distribution is centered on a normalized radius r/a~0.15, corresponding in that case to the position of the ion cyclotron resonance layer, with an effective temperature ($T_{eff}=(T_{//}+2T_{perp})/3$) strongly decreasing with increasing n_H/n_e (figure 1-b). The fast ion tail does not extend beyond the normalized radius r/a=0.35 and the hydrogen temperature out of this limit is the temperature of the background ions. The temperature anisotropy $T_{perp}/T_{//}$ also decreases from 4.5 at low concentration (n_H/n_e=1%) to 1.2 at high concentration (n_H/n_e=15%) (Figure 2-a).

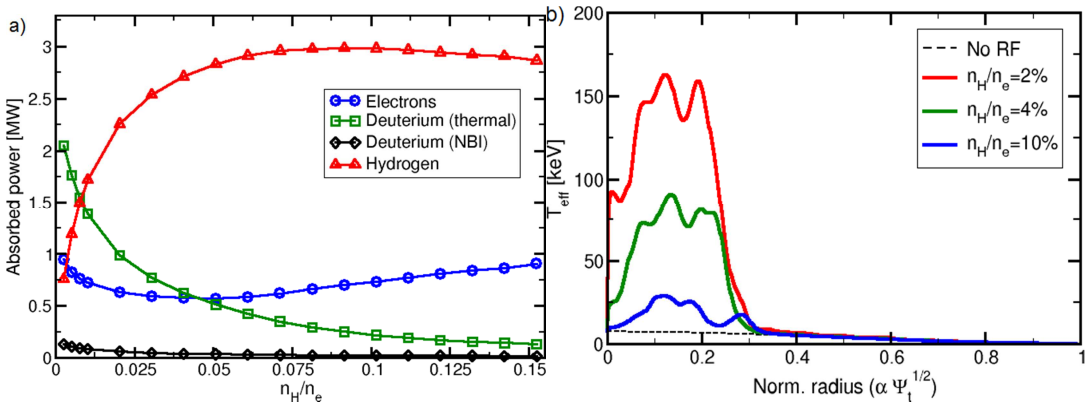

Figure 1 a) Wave power damping on the different species b) Radial profile of the effective temperature ($T_{eff}=(T_{//}+2T_{perp})/3$). $P_{NBI}=24MW$, $P_{ICRH}=4MW$, $n_e(0)=6.5\times10^{19}m^{-3}$, $T_e(0)=7.5keV$, $T_i(0)=7.5keV$ (parameters identical to those of the hybrid pulse 87253, $B_t=2.9T$, $I_p=2.5MA$).

Collisional redistribution of the absorbed power to the D ions increases when n_H/n_e increases from 4% to 12% and then levels off for larger concentration. This mostly results from the increasing thermal contribution to the total hydrogen ion energy as the minority concentration increases. As a consequence, the total power absorbed by the electrons in the core plasma (r/a<0.25) decreases from 1.6MW (40% of the total power) to 1.0MW (25% of the total power) when the H concentration is increased from 3% to 10% (Figure 2b). The ratio of the power transferred to the electrons in the whole plasma varies in a more limited range (45-55%). Experiments carried out with hydrogen minority concentration varying between 2% and 23% (Van Eester 14, Lerche14) show that when n_H/ne is increased from 2% to 15%, the central electron temperature decreases by 20% when the ion temperature, deduced from the neutrons rate, decreases by only 12%, indicating a relative increase of the power damped on the deuterium ions at high H concentration but this power does not increase with this concentration as a result of weaker absorption of the wave. In the experiments, the power fraction going to the electrons is significantly more important than expected from modelling at low concentration (n_H/n_e=2-3%). This could be the result of the additional electron heating provided by the fast deuterium population which is not taken into account in this modelling. The observed slight increase of W peaking when the minority concentration is increased is therefore qualitatively correlated to the decrease of electron and ion temperatures.

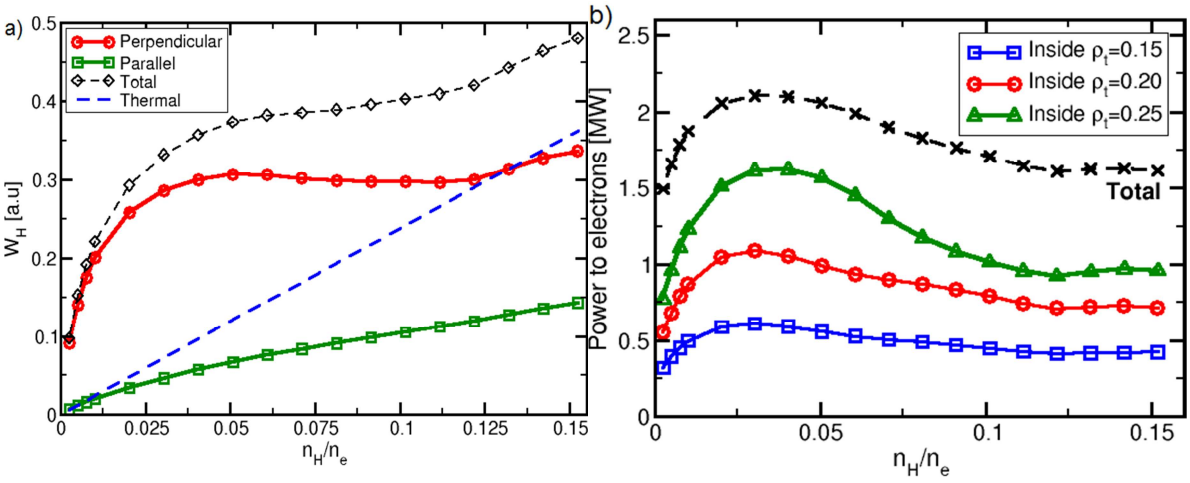

Figure 2 a) Energy in the perpendicular and parallel degrees of freedom of the hydrogen ions b) Fraction of RF power transferred to the electrons and ions after collisional redistribution (solid lines) and fraction of the power transferred from the hydrogen to the as a function of the minority concentration n_H/n_e. P_{NBI}=24MW, P_{ICRH}=4MW, $n_e(0)=6.5\times10^{19}m^{-3}$, $T_e(0)$=7.5keV, $T_i(0)$=7.5keV.

From the modelled fast ion temperature profile, the temperature screening factor $n_f T_f^{-1/2}(R/L_{Tf})$ was computed and compared to the temperature screening factor provided by the thermal deuterium ions. This screening factor is found to be the highest at r/a~0.28 for the low range of hydrogen concentration (3%<n_H/n_e<10%) and the maximum moves inwards for higher concentrations (figure 3). For the usual cases of ICRH with n_H/ne <10%, the screening provided by the fast H ions is much lower (at least a factor 3) than that provided by the thermal D ions. The screening by fast ions and thermal ions, with n_H/ne=9%, was found of the same order in a previous work [Casson 2015]. Taking into account, the large uncertainty on the temperature gradient dT_f/dR for the calculation of the screening factor, the screening factor has an error bar of at least ±30% but surely this factor increases with n_H/ne although the temperature of the fast ions sharply decreases. However, experimentally the peaking of tungsten concentration is observed to be the lowest for n_H/n_e~2% when the screening factor by the fast ions is the lowest and we conclude that screening of W by the ICRH fast ions plays a minor role in these experiments.

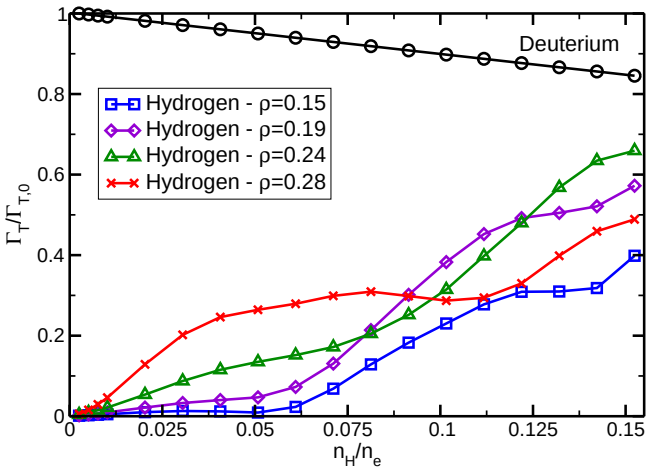

Figure 3. Temperature screening factor Γ_T normalized to the case of a pure D plasma $\Gamma_{T,0}$ for fast H and thermal D ions (same plasma parameters than figure 2).

3. Effect of the ion cyclotron resonance position and MHD activity.

In order to optimize the heating scenario, the ion cyclotron resonance position (R_{IC}) was varied either by ramping the toroidal field at constant current (Ip=2.5MA) [Lerche 14] or by ramping both the toroidal field and the plasma current at constant safety factor (q_{95}=3.5) [Graves 15]. The ICRH power was in the 3.2-3.8MW range when the total injected power (NBI+ICRH) lied between 19MW and 22MW. The hydrogen concentration was relatively high for the Ip-constant discharges (X[H]=7-9%) and low for the q-constant discharges (X[H]=3-5%).

Central electron temperature, measured before the sawtooth crash, increases from ~4keV to ~5.5keV when the IC resonance layer is moved from the high field side (R_{IC}-R_{mag}=-0.15m) to the low field side (R_{IC}-R_{mag}=0.20m). For the highest temperature (T_e>5keV), a 1.3s long sawtooth-free period is obtained (Fig.4-a). In the case of the q-constant discharges, the IC resonance position is scanned on the low-field side from R_{IC}-R_{mag}=0.35m to R_{IC}-R_{mag}=0.10m, except for pulse 85084 which has stationary plasma parameters. Central temperature is found to be maximum for R_{IC}-R_{mag} = 0.05-0.2m, depending on the scenario. For the same discharges, the normalized logarithmic gradient of the temperature R/L_{Te}, measured at r/a=0.2, is also maximum for R_{IC}-R_{mag} = 0.10-0.20m and falls off very rapidly when the resonance layer is further out (Fig.4-b). Within the uncertainty on the magnetic reconstruction, this drop could be related to the point where the

ICRH resonance crosses the q=1 surface. The ion temperature gradient R/L_{Ti}, measured at r/a~0.35, also increases from ~2 to ~4 when R_{IC}-R_{mag} increases from -0.15m to +0.20m. Surprisingly, the normalized logarithmic gradient of the density R/L_n, increases monotonically from ~0.5 to ~1.5 when the IC resonance is moved from the HFS to the LFS. The sawtooth-free discharge has a slightly higher density gradient.

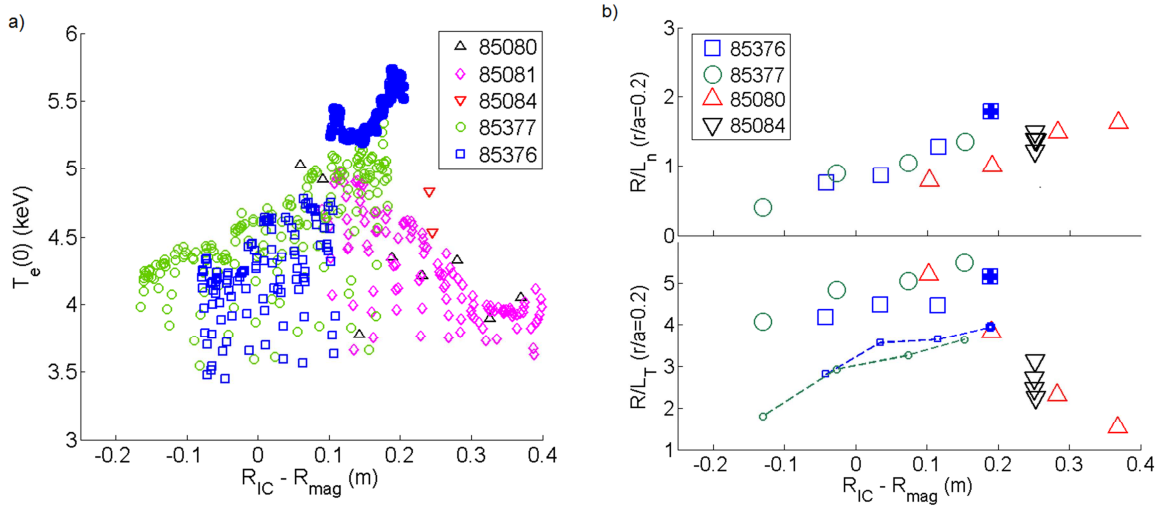

Figure 4 a) Central electron temperature b) Normalized density and temperature gradients as a function of the IC resonance layer position. Electron temperature (large symbols) and ion temperature gradients (small symbols, dashed lines) are measured at r/a=0.2 and 0.35, respectively. The normalized gradients are obtained from profiles averaged on 1-second time slices. The close symbols are for the 1.3s long sawtooth-free period. The q=1 surface on the low field side is located at a distance from the magnetic axis $R_{q=1}$-R_{mag}≈0.26m. Pulses 85080 and 85081 have constant safety factor (I_p=2.5-2.8MA, B_t=2.75-3.1T), 85376 and 85377 have constant I_p (I_p=2.5MA, B_t=2.6-2.9T), pulse 85084 (∇ symbols) constant B_t and I_p.(I_p=2.6MA, B_t=2.9T), P_{ICRH}=3.2-3.9MW.

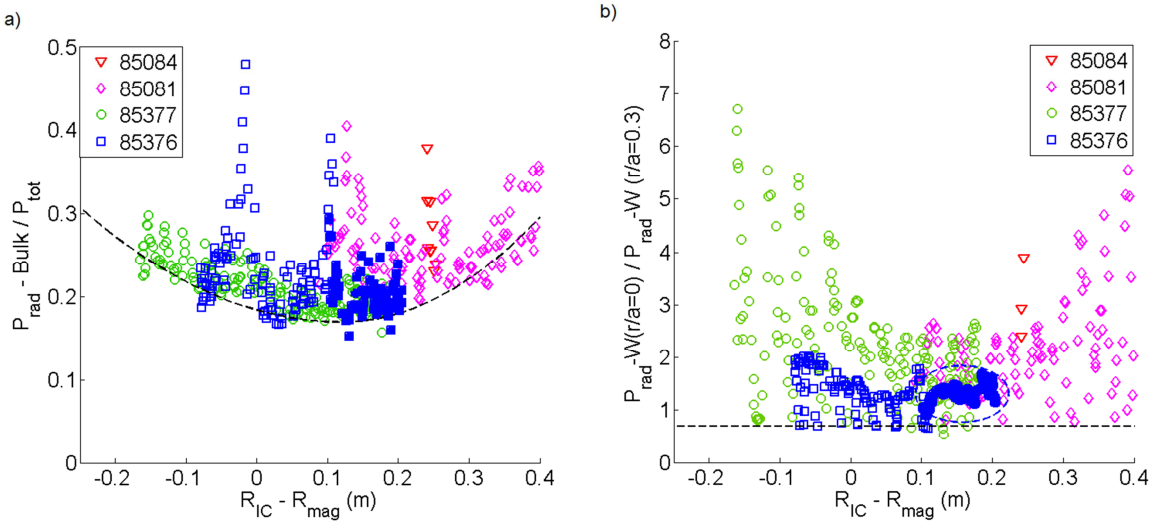

Figure 5 a) Fraction of the input power radiated in the main chamber (frombolometry) b) Peaking of the radiated power density as a function of the IC resonance position (from SXR). The close symbols are for the 1.3s long sawtooth-free discharge. The pulse 85084 (Δ symbols) has constant B_t/I_p.

The fraction of radiated power in the main chamber (P_{rad}-Bulk/P_{tot}) and the peaking of the tungsten radiation ($PF_{0.3}$=P_{rad-W} (r/a=0)/P_{rad-W} (r/a=0.3) are both minimized when the IC resonance position is such that R_{IC}-R_{mag} lies between 0 and 0.20m (figure 5). The absolute value of tungsten radiation at r/a=0 is also the lowest for this range of IC resonance position (0.05-0.1MW/m^3). After the sawtooth crash, the tungsten peaking drops to ~0.7 hollow profile) for any resonance position (dashed line of fig. 5-b). It is noticeable that despite a significant peaking of the density, the sawtooth free discharge has low radiation and low tungsten peaking (~1.5). These quantities do not evolve significantly during this 1.3s long phase of the discharge and are kept close to the minimum. Using the proxy for neoclassical flux (section 1, page 9), this could be interpreted as the lack of sawteeth and the slight density peaking are counterbalanced by the high temperature peaking ($R/L_{Te} \approx 5$ at r/a=0.2, R/L_{Ti}~4 at r/a=0.35) to flush out the tungsten. Sawtooth free discharge has also been obtained by reducing the hydrogen minority concentration to ~2% and, although the core radiation increases very slightly, the core tungsten concentration is maintained below 10^{-4} for 3.5s [Van Eester14, Goniche 14].

It should be noted that, at mid-radius (r/a=0.5), tungsten concentration is observed to vary by no more than ±25% for these pulses, as nickel concentration, derived from the VUV NiXXV line intensity [Czarnecka 14].

It appears that by setting the resonance layer on the low field side, inside but near the q=1 surface, the tungsten accumulation can be minimized in the baseline scenario. This is a quite favorable situation as sawtooth control requires also off-axis heating [Lennholm 15, Graves 15].

In addition to the sawtooth instability, other MHD modes are expected to act on the tungsten transport [Nave 2003, Pütterich 2013, Angioni 2014]. When the large sawtooth (ΔTe=1.5keV) occurs after the 1.3s long sawtooth free period (#85376), a (m=3, n=2) neoclassical tearing mode (NTM) is destabilized for the rest of the discharge (f=9-10kHz) whereas a m=1, n=1 internal kink mode (f=8-9kHz) is present during the other pulses (#85377 &85081). The NTM does not seem to foster tungsten accumulation (tungsten

peaking just increases transiently from ~1.3 to ~1.7) when for the same IC resonance position, the tungsten peaking of the pulse with the (1, 1) mode (#85377) has indeed a higher tungsten peaking. Whereas NTM modes often accelerate the W accumulation (Angioni 14, Hender 16], here the weak effect of the mode is the result of the weak off-axis tungsten concentration ($<10^{-4}$). In both cases, fishbone modes with quite a large frequency span (f= 5-9kHz for 85376, f=7-11kHz for 85377, f=8-13kHz for 85081) are destabilized when the IC position is on the LFS, close to the magnetic axis ($0<R_{IC}-R_{mag}<0.15$m) (figure 6).

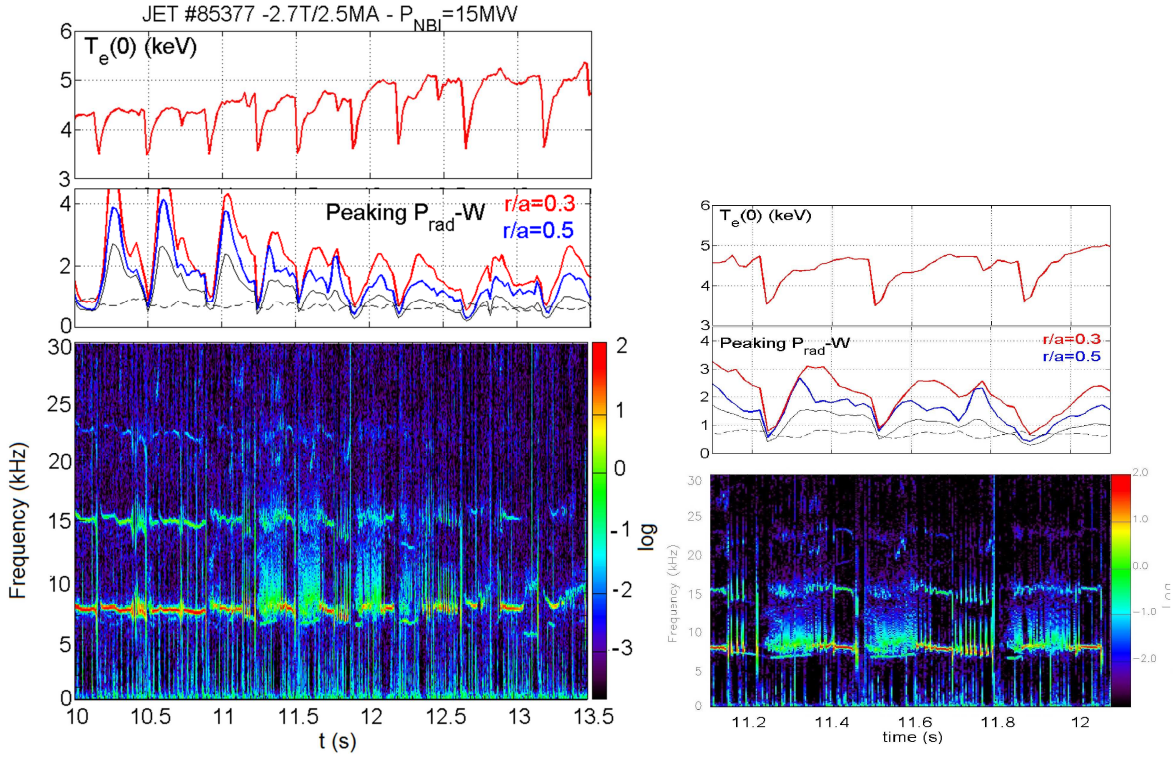

Figure 6. Central temperature, tungsten radiation peaking $P_{rad}(r/a=0)/P_{rad}(r/a=0.3)$ (red line), $P_{rad}(r/a=0)/P_{rad}(r/a=0.5)$ (blue line), tungsten radiation $P_{rad}(r/a=0)$ (10^5W/m^3, black solid line), $P_{rad}(r/a=0.5)$ (10^5W/m^3, black dotted line), spectrogram (from magnetic loops). Magnetic field is ramped up during this discharge. $R_{IC}-R_{mag}=0$ at t=11.0s and $R_{IC}-R_{mag}=0.13$m at t=12.5s ($P_{ICRH}=3.8$MW). Fishbone activity can be seen at t=11.25-11.4s, 11.5-11.6, 11.85-12.0.

This fishbone activity, which appears in the form of rapid chirps between about 13 kHz and about 8 kHz and does not last more than 100-150ms, alternate with a continuous mode at about 8kHz. This evolution should be the result of a modulation of the fast ion pressure gradient from high values (shortly after the sawtooth crash) to lower value which gives an internal kink gap mode [Breizman 2011]. In that case, core tungsten radiation has actually a 3-step cycle. Starting from the sawtooth crash, there is a fast and short flattening of the

radiation profile, followed by peaking lasting 100-200ms and finally the core profile flattens again for 200-300ms until the next sawtooth crash (figure 6).

4. ICRH in JET Baseline scenario

4.1 Medium plasma current experiments

ICRH power varying between 0 and 6MW was coupled to 2.7T/2.5MA discharges with total power close to 20MW at a frequency of 42.5MHz providing central heating with the IC resonance layer located about 5cm from the magnetic axis on the high field side in most cases.

The first series was performed with the outer strike point on the tile 5 of the bottom divertor (R_{OSP}~2.73m) and gas rate in the range of 0.9-1.2×10^{22} el./s . This allows to be well above the L-H transition and to get type I ELMs with frequencies in the 30-45 Hz range. For the same total power (19-20MW), when the ICRH power is increased from 0 to 6MW, a strong decrease of the tungsten radiation in the very core (r/a~0) from 0.2MW/m^3 to 0.07MW/m^3 is observed and the W radiation peaking decreases correspondingly from ~10 to ~1.5 (figure 7-a). A weaker decrease is observed further out in the plasma volume and at r/a~0.45, radiation per unit volume starts increasing and decreases when the ICRH power exceeds 4-5MW. The same trend is observed for the nickel concentration and for the total radiated power from bolometry. The LFS/HFS asymmetry of the SXR radiation can be estimated from the ratio of the raw signals given by the lines of sight tangent to the same magnetic surface. This was done at r/a=0.3 and interpolation from the 2 nearest lines of sight was carried out for better accuracy (figure 7-b). This asymmetry decreases from 3.5-4 (P_{ICRH}=0) to 1.8 (P_{ICRH}~4.5MW) for the low gas rate case. This effect could the result of the reduced toroidal rotation when adding ICRH (the NBI power is reduced by 20-30% to keep the total power constant) but the impact of ICRH on the asymmetry is too strong to be only caused by the change of toroidal rotation and the stronger temperature anisotropy of the hydrogen when the ICRH power is increased is very likely also the cause of reducing the radiation asymmetry. As an effect of the reduced contamination of the plasma core by high-Z impurities, the energy confinement, evaluated from the $H_{98y,2}$ factor, slightly increases from ~0.72 to ~0.77, when

correction for the ICRH fast ion contribution to the plasma diamagnetic energy was applied.

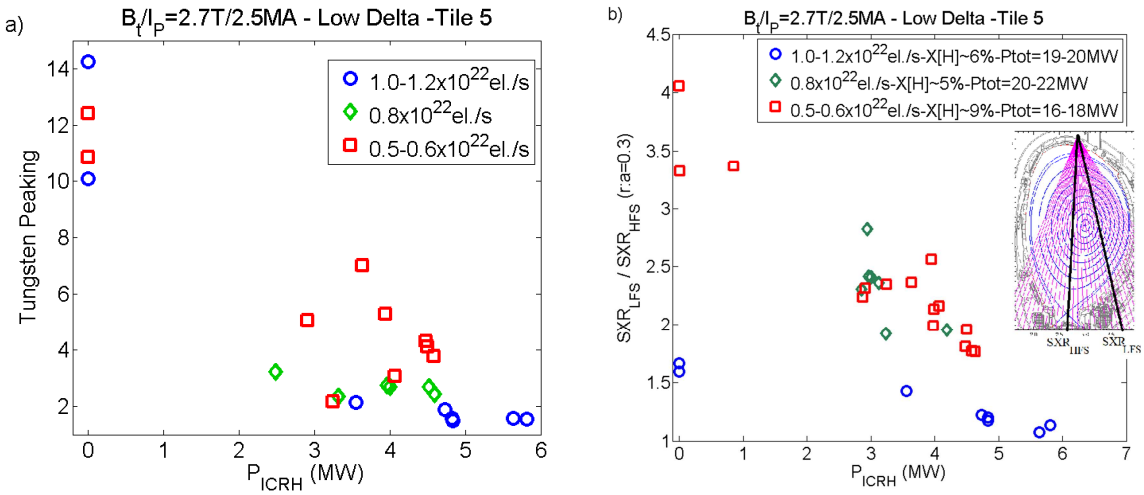

Figure 7 a) Radiated powers (total from the bulk of the plasma and from tungsten at different radii, flux surface-averaged). b) asymmetry of the SXR radiation in the mid-plane at r/a=0.3. Nearest tangent line-of –sight is chord 13 (HFS) and 23 (LFS). Data collected at least 2seconds after the start of the high power phase

At low gas rate (~0.5×10^{22} el./s), the ELM frequency decreases to 15-20Hz and both the total radiation and core tungsten radiation increase strongly. P_{rad}-bulk/P_{tot} is still above 45% and P_{rad}-W(r/a=0) above 0.4MW/m^3 with 4.6MW of ICRH power. However the SXR radiation asymmetry decreases linearly with power from ~4 (P_{ICRH}=0) to ~1.8 (P_{ICRH}=4.6MW) (figure 7-b).

Comparing, the evolution of a 4-s long high power phase with low (0.5×10^{22} el./s, #84492) and medium (1.1×10^{22} el./s, #85379) gas rate and same ICRH power (~4.6MW), these discharges have same sawtooth period (~380ms) and slightly higher central electron temperature (due to higher NBI power) for the medium gas dosing case (Figure 8). The tungsten is expelled from the core (r/a<0.2) during the sawtooth crash and a quasi-periodic regime is established for the tungsten radiation with no trend of further increase on a long time scale. It should be noted that, although the central radiation is higher by a factor ~6 and the total radiation by a factor 2.5 for the low gas dosing discharge, the confinement is improved and the H-factor increases from ~0.79 to ~0.85, thanks to the higher pedestal pressure.

When the outer strike point is moved closer to the pumping duct (R_{OSP}~2.92m), with higher gas dosing (1.7×10^{22} el./s), high ELM frequency (~100Hz) is combined with low radiation (P_{rad}/P_{tot}~20%, P_{rad}-W(0)~0.06MW/m^3) and similar confinement ($H_{98,y}$~0.85) to that of the low gas dosing case with low pumping (R_{OSP}~2.75m) is obtained.

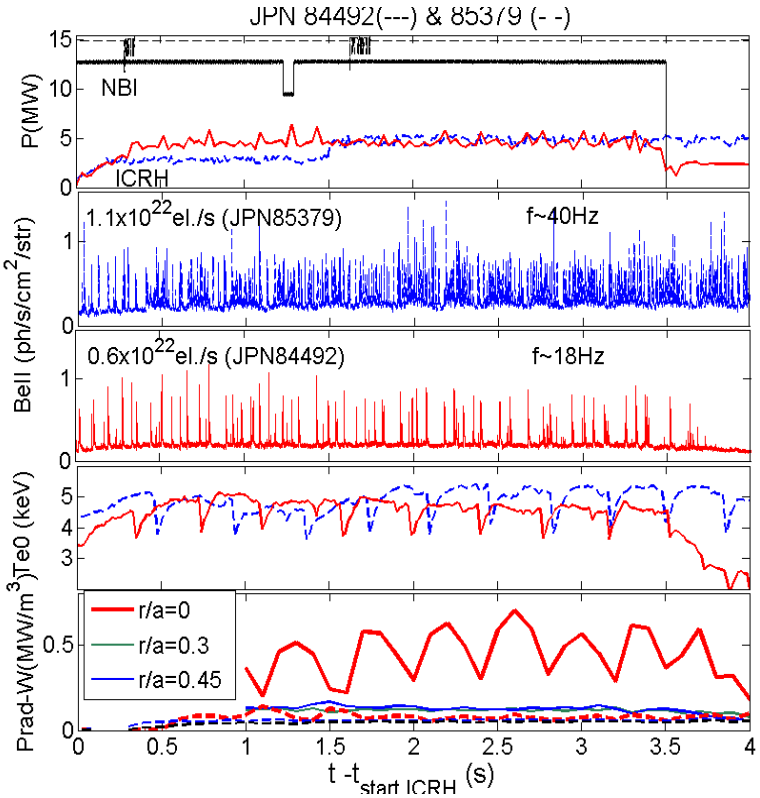

Figure 8. Effect of gas rate on ELMs frequency, $T_e(0)$ and tungsten radiation (from SXR diagnostic). B_t=2.7T, I_p=2.5MA, $n_e(0)=7.1\times10^{19}$ m^{-3}.

For all gas dosing and pumping cases, the normalized logarithmic gradient of the electron temperature R $(dT_e/dR)/T_e=R/L_{Te}$, increases from ~2 to ~5 when the ICRH power increases from 0 to 6MW (figure 9). The equivalent quantity for the density, R/L_n, decreases with the ICRH power from ~1.5 to ~0.5 for the low pumping case. In the case of high pumping and high gas dosing, the central density is significantly lower ($n_e(0)$~6×10^{19} m^{-3}) compared to the low pumping case ($n_e(0)$~7×10^{19} m^{-3}) with 4MW of ICRH power and the normalized logarithmic gradient is higher (R/L_n~2).

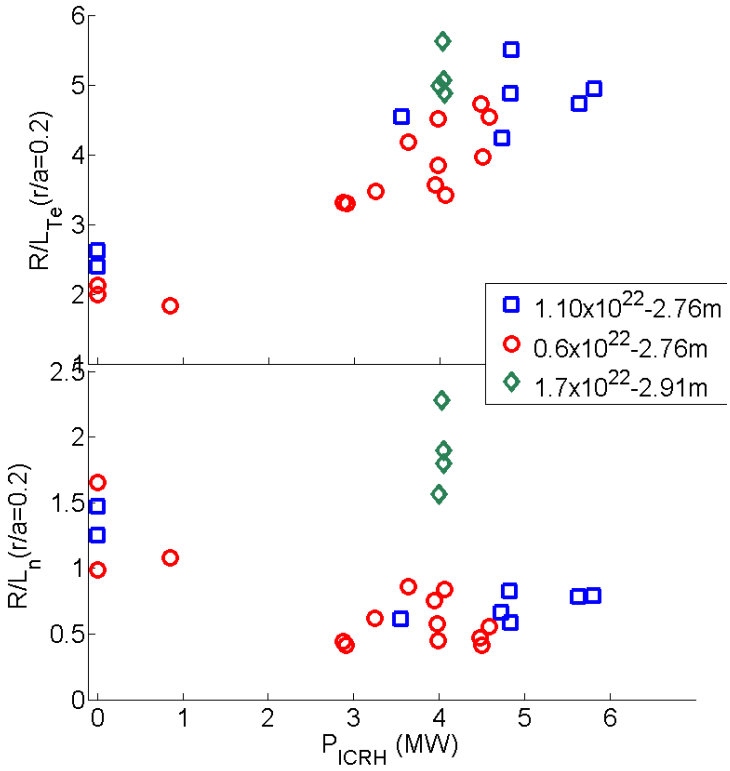

Figure 9. Normalized gradient lengths at r/a~0.2 for various gas rates (0.6, 1.1 and 1.7×10^{22} el./s), and strike point positions on the outer divertor (2.76m and 2.91m).Total power is in the 18-20MW range. The ELM frequency is 15-20, 30-45, 90-100Hz for, respectively, the 0.6, 1.1, 1.7×10^{22}el./s cases.

When comparing the low density/low gas dosing discharge (circle symbols of figure 9) to the high gas dosing discharge (diamond symbols) with the same ICRH power (4MW), $R/L_{ne} - 0.5R/L_{Te}$ is negative, close to -1, for the former and close to -0.5 for the latter. However, the tungsten peaking evaluated from $PF_{0.3}$ is found to be quite high ($PF_{0.3}$=2-7), for the low gas rate case and low ($PF_{0.3}$ =1.3-2) for the high gas rate case.

The tungsten radiation peaking was estimated for a large data base including pulses with various P_{tot} (15-20MW), P_{ICRH} (0-6MW), minority hydrogen concentration X[H] (2-20%). A good correlation between $R/L_{ne} - 0.5R/L_{Te}$ and the tungsten peaking which is varying between 1 and 14 (figure 10) is found. The beneficial effect of ICRH on the gradients is clearly observed and the sign of convection is inverted from inward to outward for an ICRH power exceeding 3MW for most cases. However, as mentioned in the previous paragraph, a significant difference is observed between low gas rate/low pumping pulses (+ symbols of

figure 10) and high gas rate/high pumping pulses (× symbols of figure 10): although they have almost the same $R/L_{ne} - 0.5R/L_{Te}$ value, higher peaking of the tungsten radiation is observed for the low gas rate pulses. In that case we may expect a net higher tungsten influx from the edge resulting from the lower ELM frequency [den Harder 16] but also possibly from the higher RF rectified sheath, caused by the higher antenna electric field (the antenna coupling resistance is lower by 20-25% in this case) [Colas 06, Jacquet 13]. Consistently, the core tungsten radiation is about 10 times higher when compared to the high gas rate cases.

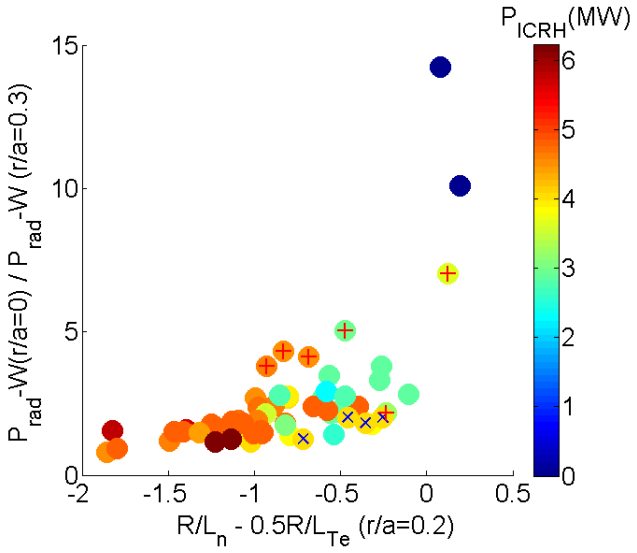

Figure 10. Tungsten radiation peaking (from SXR measurements) as a function of $R/L_{ne} - 0.5R/L_{Te}$. Electron densities are provided by the LIDAR diagnostic, the electron temperature by the ECE diagnostic. Low gas rate/low pumping (+) and high gas rate/high pumping (×) cases of figure 7 are highlighted. Data are averaged on a 1-second time window, at least 1 second after the start of the ICRH power. B_t=2.7T, I_p=2.5MA.

4.2 High Plasma current experiments

During the recent development of the baseline scenario, in preparation of the D-T campaign, the plasma current was increased from 2.5 to 4.0MA while keeping q_{95} close to 3 (B_t=2.7-3.7T) [Nunes 2014]. The outer strike point was close to the pumping duct (R_{OSP}~2.92m) and the gas injection rate was increased with respect of the lower plasma experiments (2-5×10^{22} el./s). The total power was varied between 15MW and 30MW and the ICRH power was in the 2-5MW range. The position of the IC resonance layer is constrained by the scenario and the available bands of frequency of the ICRH generators. As a consequence the position of the IC resonance layer was varied such as $0<R_{IC}-R_{mag}<0.40$m.

At 3.0MA with medium gas injection (~3×10^{22} el./s), leading to a high ELM frequency (~100Hz), the maximum core tungsten peaking increases regularly from one sawtooth cycle to the next one (figure 11-a), exceeding 4, at 3 seconds after the start of the ICRH power (P_{ICRH}=4.5MW). The W peaking (and the absolute radiated power at the center) is also strongly modulated with the sawtooth period but the flat tungsten profile (peaking =1) is achieved now just before the sawtooth crash: instead of the 3-step cycle described for 2.5MA discharges (see section 2), tungsten in the plasma center exhibits now a 2-step cycle. In this case the peaking increases with T_e after the sawtooth crash and decreases, until the next sawtooth crash, when T_e is stationary or even slightly decreasing as observed between t=9.7 (resp. 10.25s) and 10.1s (resp.10.65s). The peaking increase is accompanied by fishbone activity with low amplitude and a large frequency span (between 10 and 15kHz). This is followed, during the W radiation flattening phase, by fishbones with smaller frequency span and large amplitude. The (1,1) kink mode alternating with the fishbones is growing in amplitude until the next sawtooth. For a pulse performed with the same conditions (including same IC resonance position) but with higher magnetic field (q_{95}=3.6), the amplitude of the fishbones is smaller and the flattening of the tungsten radiation profile is weaker (figure 11b).

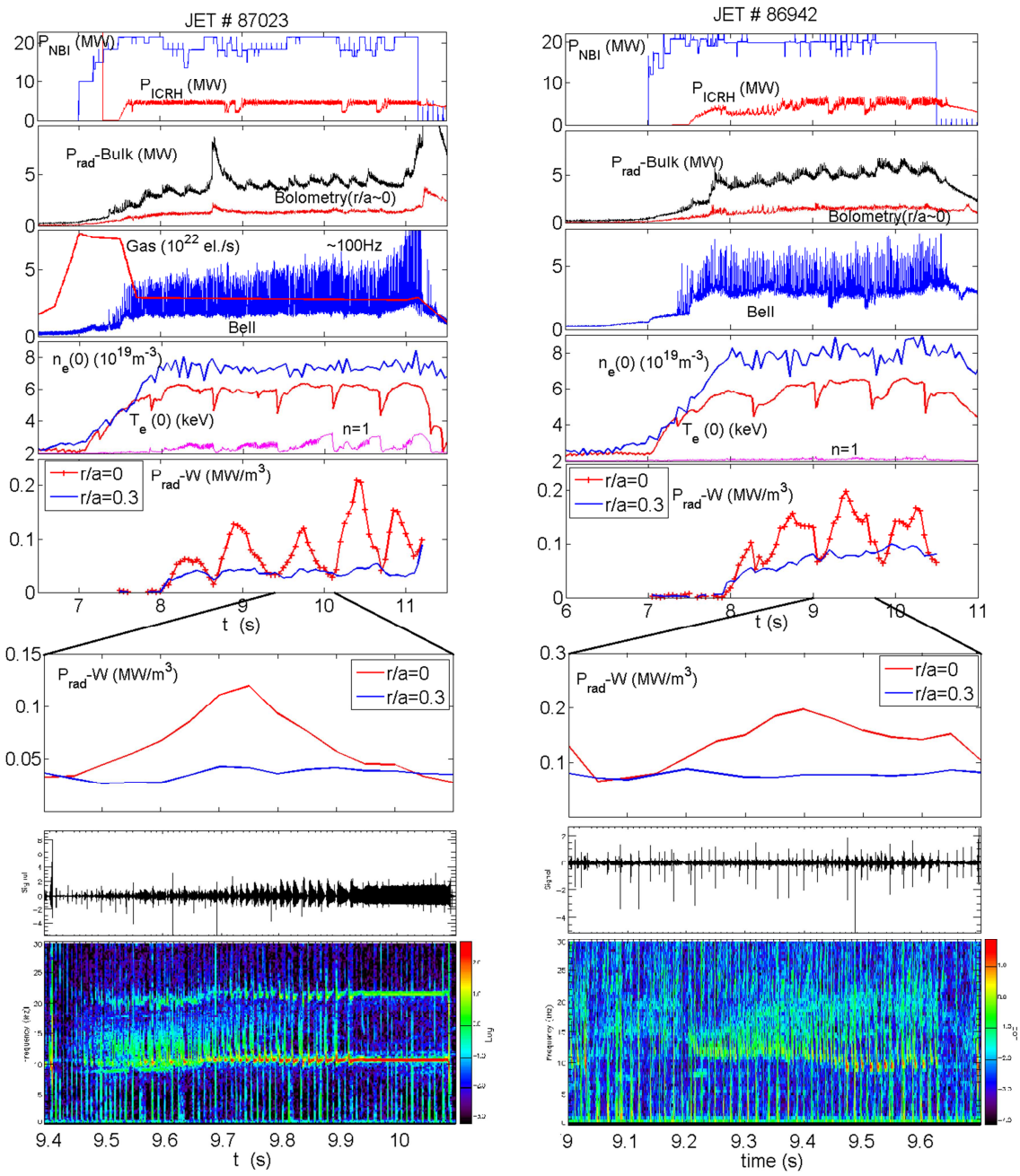

Figure 11. Time traces of 3MA discharge a) 87023 (q_{95}=3.0) b) 86942 (q_{95}=3.65). For both pulses: P_{NBI}≈20MW, P_{ICRH}≈4.5MW, R_{IC}-R_{mag}=0.10m, X[H] ≈5%. A blow-up of the tungsten radiation between two sawtooth crashes and the corresponding spectrogram from a magnetic pick-up coil are displayed in the bottom of the figures. The scale of the spectrogram of discharge 86942 is reduced by a factor 10.

An example where the IC resonance is moved out of the q=1 surface (R_{IC}-R_{mag} =0.39m) is shown in figure 12. Although the gas rate is strongly increased (~5×10^{22} el./s), while maintaining the same ELM frequency (~100Hz), peaking of the tungsten radiation now increases to very high values (10-20) until the sawtooth crashes, then the radiation

profile gets flat with a peaking close to 1. No fishbone activity, but a strong continuous (1,1) mode, is triggered by ICRH fast ions as the trapped ions are now mostly out of q=1 surface.

It should be noted that, when comparing discharges with same q_{95} but resonance inside (#87023) and outside (#87380) the q=1 surface, the tungsten radiation at the center (r/a~0) just increases from ~0.1MW/m^3 to ~0.15MW/m^3 when this quantity is averaged on a sawtooth period. The total powers radiated from the bulk plasma are also very similar with P_{rad}-Bulk/P_{tot}~0.16-0.18, which are lower ratios than those obtained at 2.5MA for which P_{rad}-Bulk/P_{tot}~0.18-0.21 The density normalized gradients are very similar for these pulses (R/L_n~1) but the temperature gradient is higher when the resonance is central (R/L_{Te}~4 vs 2.5). Ion temperature, measured at r/a~0.4, is also much higher (factor ~1.4), in rough agreement with the neutron yield (factor ~1.6), for the central heating case. It results a $R/L_{ne} - 0.5R/L_{Te}$ value lower for central heating (~-1) than for off-axis heating (~0) when the average tungsten peaking varies between 2 and 3 for the first case and 6 and 7 for the second one. These data (peaking vs $R/L_{ne} - 0.5R/L_{Te}$) fit those obtained at 2.5MA with low gas rate /low pumping (+ symbols of figure 10).

When the current is further increased to 3.5MA with quite low gas injection (~2 $\times 10^{22}$ el./s) and low ELM frequency (~40Hz), the radiated power increases strongly (P_{rad}-Bulk/P_{tot}~0.4-0.45) and the maximum tungsten peaking increases during the 3-second high power phase up to ~10. At the same time the core tungsten radiation exceeds 0.7MW/m^3. The maximum of W radiation peaking (and the maximum core radiation) is now observed only ~100ms after the sawtooth crash (t_{ST}~600ms). Off-axis ICRH heating (R_{IC}-R_{mag}=0.40m), with higher gas injection (~3.5 $\times 10^{22}$ el./s) and slightly higher ELM frequency (~50Hz) leads to a strongly peaked tungsten profile, with a peaking factor exceeding 10, just before the sawtooth crash as observed at a plasma current of 3MA. The normalized density and temperature gradient lengths, averaged over one second, both flatten weakly when going from 3.0MA to 3.5MA and the $R/L_{ne} - 0.5R/L_{Te}$ quantity is unchanged (~-1) for the central ICRH heating scenario. This is roughly consistent with the W radiation peaking, averaged over one second, which increases only from ~2 to ~3, 1.5s after the start of the ICRH power. In the case of the off-axis ICRH, $R/L_{ne} - 0.5R/L_{Te}$ ~0 for the two values of plasma current when the averaged W radiation peaking is ~9 at 3MA and ~5 at 3.5MA, 2s after the start of the ICRH power.

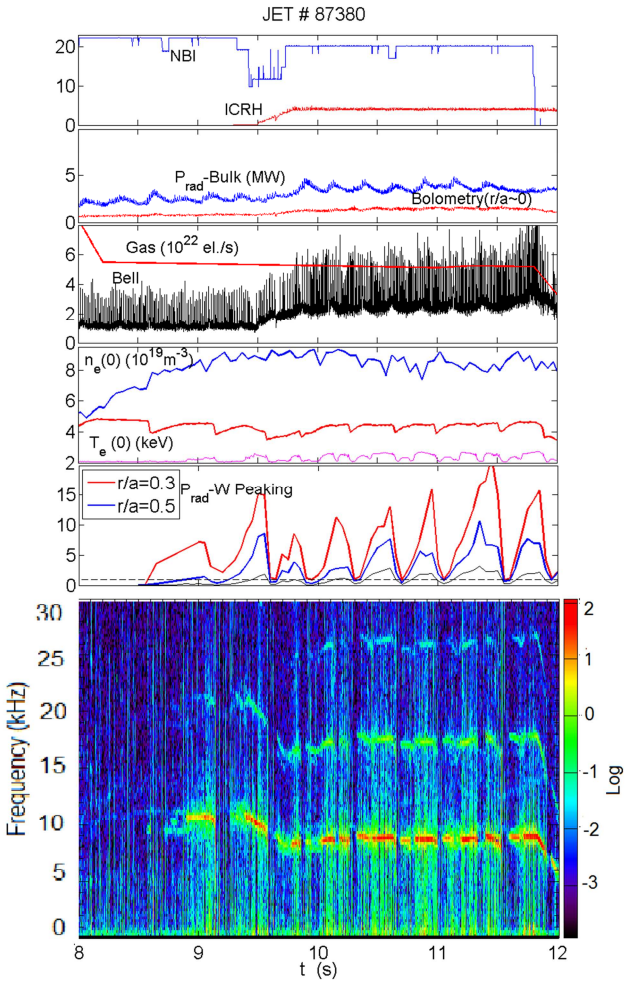

Figure 12 Time traces of 3MA/2.95T discharge 87380 (q_{95}=3.0) with P_{NBI}≈20MW, P_{ICRH}≈4MW, R_{IC}-R_{mag}=0.39m, X[H] ≈7%.

As a conclusion, when the current is increased from 2.5MA to 3.5MA with q_{95}~3, the maximum of tungsten peaking increases after 2-3 seconds of high power phase (P_{tot}~24-27MW) with central ICRH heating (P_{ICRH}~4MW), from ~2 to ~10 (~4 at 3MA). At the same time, core (r/a~0) tungsten radiation increases from ~0.1MW/m^3 (n_W~10^{-4}) to ~1MW/m^3 (n_W~10^{-3}). At high plasma current (I_p=3-3.5MA), tungsten peaking and core tungsten radiation are the highest 100-300ms after the sawtooth crash and decrease later until the next sawtooth crash. This increase and decrease of tungsten peaking is correlated with fishbone activity as follows. In the peaking phase, modes with chirping frequency typical of fishbone activity when the fast ion pressure gradient is large are detected [Breizman 2011]. During the flattening phase, this fishbone activity gets weaker, a continuous frequency (~10kHz) mode, identified as the (1,1) internal kink , alternating with the weak fishbones, grows and

eventually the fishbone activity vanishes. This gap mode is typical of a low fast ion pressure gradient. When the IC resonance is moved out of the q=1 surface on the low field side, the amplitude of the sawtooth activity is reduced, the fishbone activity is suppressed, but a strong (1,1) mode accompanies the strong increase of the tungsten peaking which now exceeds 10 very shortly after the start of the high power phase.

Beneficial effect of ICRH above 3-4MW on tungsten peaking is confirmed. However, at moderate gas injection (1-2×10^{22} el./s), there is a significant increase of the tungsten peaking at high plasma current (Ip=3.0-4.0MA) with respect of the peaking obtained at lower current (Ip=2.5MA)(figure 13).

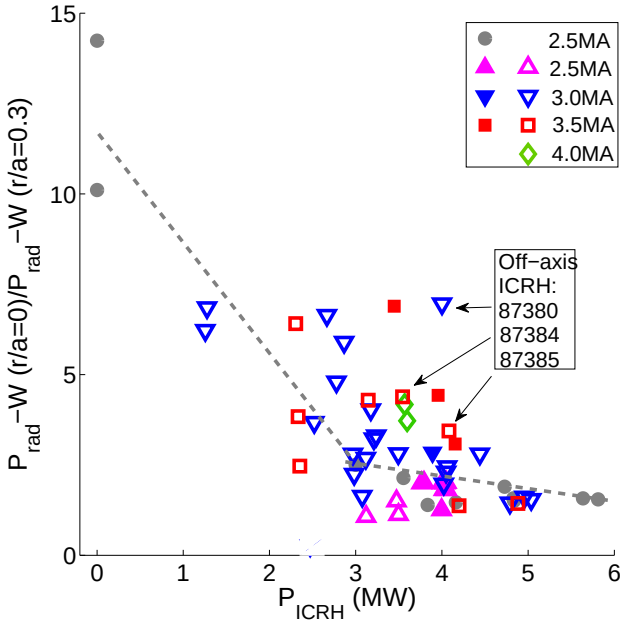

Figure 13. Tungsten radiation peaking at various plasma currents and ICRH powers. Closes symbols are for low to medium gas rate discharges (1-2×10^{22} el./s, open symbols for high gas rate discharges (2.3-5×10^{22} el./s). Low pumping discharges (see figure 7) are indicated with a circle symbol. Off-axis ICRH cases (R_{IC}-R_{mag}~0.40m) are highlighted. Radiation data ate flux surface averaged and time-averaged (Δt=1s).

A flat tungsten profile (peaking ~1.5) can be achieved at 3-3.5MA with high ICRH power (P_{ICRH}~5MW) and high gas rate (~3×10^{22} el./s at 3MA, ~4×10^{22} el./s at 3.5MA) at the expense of the global energy confinement (H98y~0.75) of these low triangularity plasmas [Beurskens 14]. More generally, a rather good correlation is found between the tungsten core radiation and the normalized confinement time (figure 14). At low plasma current (2.5MA), high H factor (H98y>0.9) is achieved with a tungsten peaking lower than 2, even with high

gas injection. At higher plasma current (3-4MA), the confinement is clearly affected by both the level of gas rate and the effect of tungsten accumulation. However for a given gas rate (see color code of figure 14), the deleterious effect of W accumulation can be identified. It should be noted that in one of these discharges, very strong tungsten radiation outside of the r/a=0.5 surface ('tungsten event') occurs with a weak increase of the core radiation (~0.05MW/m^3) and the core tungsten peaking increases from 1 to only 1.5 only. Consistently, the $R/L_{ne} - 0.5R/L_{Te}$ factor is kept negative. At a plasma current exceeding 2.8MA, the tungsten peaking factor always exceed 2 and the H factor is lower than 0.85.

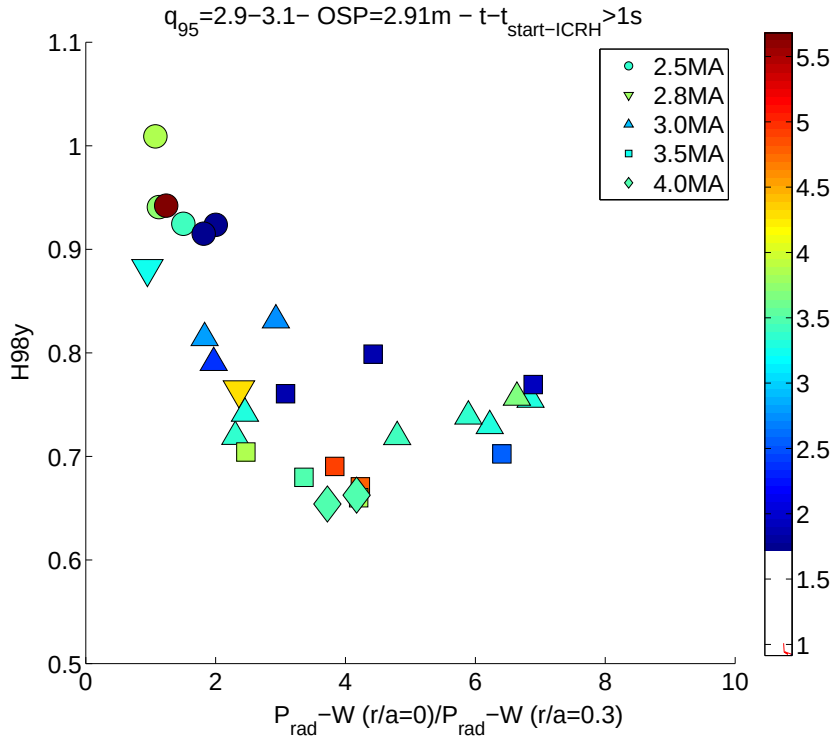

Figure 14. Normalized energy confinement as a function of the tungsten radiation peaking factor for various plasma currents for discharges with high pumping (R_{OSP}=2.91m) and low safety factor (q_{95}=2.9-3.1). The color code is for the gas rate (in 10^{22}el./s). Data are averaged on a 1 second time slice.

4.3 N2-seeded discharges

ICRH was added to discharges (B_t/I_p=2.7T/2.5MA) where nitrogen was used as a radiator aiming at reducing the heat load on the divertor and improving plasma energy confinement [Giroud 15]. These discharges have been performed with the outer strike point either on the horizontal plate far from the pumping duct (R_{OSP}=2.75-2.82m) or on the vertical plate with a higher pumping speed. In the first case, ICRH (P_{ICRH}=0-4.5MW) is applied 1 second after

the NBI start (P_{tot}=18-23MW) whereas in the second case ICRH (P_{ICRH}=0-4MW) is delayed with respect of NBI (P_{tot}=18-21MW) by 4 seconds. Central IC heating (R_{IC}-R_{mag}~-0.07m) is applied for all pulses. Deuterium and nitrogen gas rates are in the range of 2.5-7×10^{22}el./s and 1.5-4×10^{22}el./s, respectively.

For both plasma scenarios, when no ICRH is applied, strong tungsten accumulation ($PF_{0.3}$~10) occurs with strong density peaking (R/L_n>2.5) which leads to a central temperature collapses (R/L_{Te}<0). With ICRH, quasi-stationary discharges are obtained with normalized density and temperature gradients quite identical to those obtained in non-seeded discharges. It results in slightly negative values of the $R/L_n - 0.5R/L_{Te}$ parameter for P_{ICRH} exceeding 3MW (figure 15-a). Consistently, the tungsten peaking factor $PF_{0.3}$ decreases from ~7 (peak value) with no ICRH to ~1.7 (averaged on two sawtooth periods) with 4.5MW of RF power (figure 15-b). The main difference between the unseeded and seeded discharges is related to the fraction of power radiated in the main plasma. For the unseeded case, P_{rad}-Bulk/P_{tot} is quite low in NBI-only heated discharges (13%), it exceeds 55% for the N2-seeded case. With 4.5MW of ICRH, P_{rad}-Bulk/P_{tot} is reduced to 30% close to the value obtained in the unseeded discharge. This ICRH-heated discharges has an H factor of 0.83, slightly larger than for the unseeded case (H98y=0.75) with quite similar ELM frequency (50Hz vs. 40Hz).

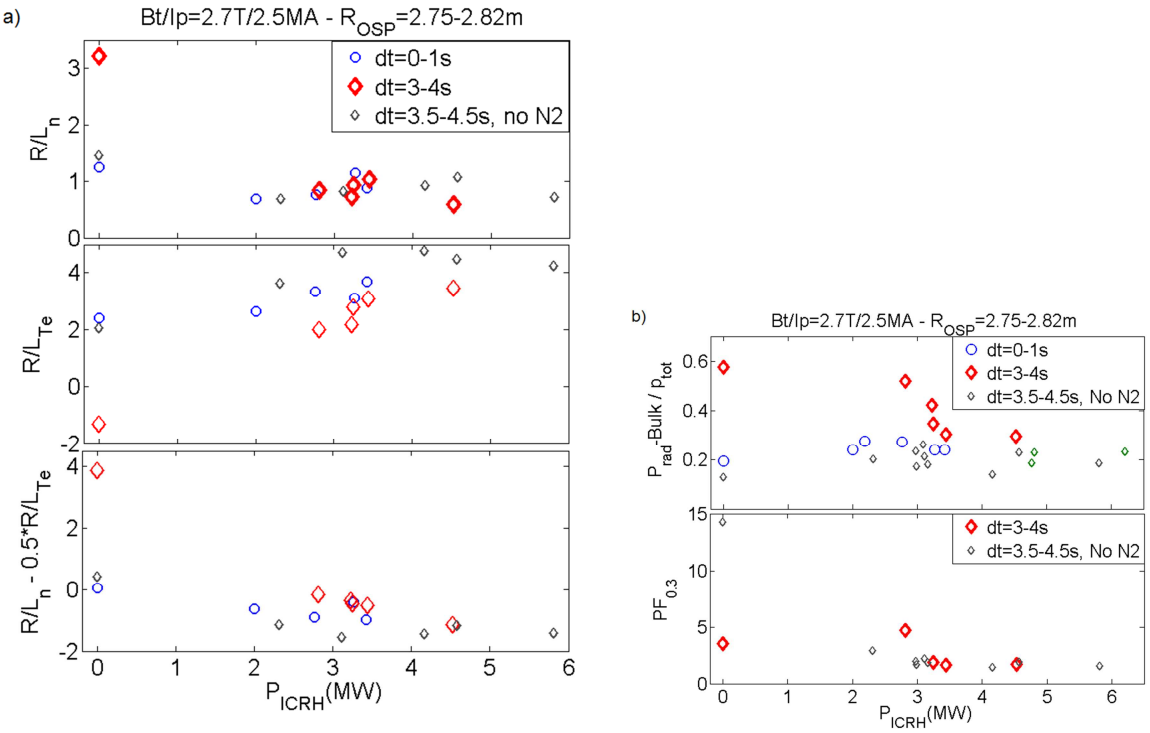

Figure 15. a) Normalized gradients b)P_{rad}/Ptot and Tungsten radiation peaking as a function of the ICRH power. P_{tot}=18-23MW, F_{tot}=6-7×10^{22}el./s, F_{N2}=3-4×10^{22}el./s, early (circles) and late (large diamonds) after the start of the ICRH power.

Similar results are obtained with the outer strike point on the vertical plate, closer to the pumping duct and tungsten peaking, averaged on 2-3 sawtooth periods, is below 2 when the ICRH power is exceeding 3.5MW. In this case with high ICRH power (>3MW), the total (resp. N2) gas rate was varied between 2.7 and 5.4×10^{22}el./s (resp. 1.5 and 3.2×10^{22}el./s). The mean tungsten peaking in stationary conditions (2-3s after the start of the ICRH power, 6-7s after the start of the NBI power) decreases from ~2.7 to ~1.8 with increasing gas rate (figure 16). At the same time the normalized density gradient R/L_n decreases from ~1.2 to ~0.4 and R/L_n-0.5R/L_{Te} from ~0 to ~-1.5. However the H-factor is found to be the highest (H_{98y}~0.9) for the low gas rate case, thanks to the highest ELM frequency (and lower ELM amplitude) providing a lower impurity source.

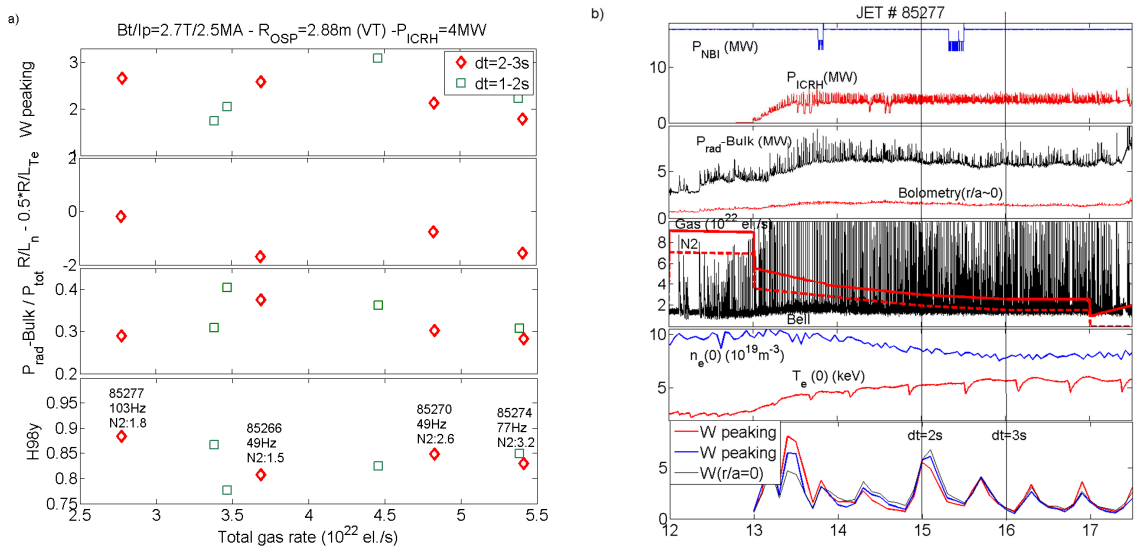

Figure 16. a) Tungsten peaking P_{rad}-W(r/a=0)/P_{rad}-W(r/a=0.3), R/L_n-0.5R/L_{Te}, fraction of radiated power and H-factor as a function of the total gas rate (P_{tot}=20MW, P_{ICRH}=4MW, outer strike point on the vertical target) at 2 time windows. The ELM frequency and the N2 gas rate (in 10^{22}el./s) are indicated for the 4 discharges. b) Time traces for the low gas rate case (2.7×10^{22}el./s). W Peaking $PF_{0.3}$ (red line), $PF_{0.5}$ (blue line) and central W concentration (in MW/m^3) are shown in the lower part of the figure. NBI starts at t=9seconds.

5. ICRH in JET Hybrid scenario

Experiments with the hybrid scenario (flat q profile with q_0~1) were conducted on JET with the ILW at I_p=2.5MA and B_t=2.9T [Challis 2015]. This scenario allows ICRH in the hydrogen minority heating scheme with R_{res}-R_{magn}=0.08-0.20m (LFS), depending on the normalized plasma pressure (β_p). In the reported experiments, the total power is in the 22-27MW range, the ICRH power in the 2.8-5.0MW range. The gas injection rate is reduced with respect of the baseline scenario (F=0.9-1.5×10^{22}el./s) aiming at achieving high confinement regime (H98y>1). However, with this scenario, the ELM frequency varies in a wide range: for F=0.9-1.2×10^{22}el./s, the ELM frequency is low (<30Hz) whereas for F>1.3×10^{22}el./s, the ELM frequency generally exceeds 70Hz with no evidence of ordering with the total input power.

The hybrid scenario is characterized by a more peaked density profile the baseline scenario. This is the generally the result of the lower collisionality of these plasmas [Angioni 2009,

Beurskens 14, Challis 15]. More particle fueling in the baseline scenario tends also to increase the density shoulder.

In order to get the required q-profile, the high power phase is generally started earlier in the discharge, typically at t=5.5s for NBI and ICRH when NBI (resp. ICRH) is started at t=7.s (resp.7.5s) in the case of the baseline scenario. As a consequence of this early timing, the initial density profile (measured just before or 1-2s after the start of the high power phase) is more peaked for discharges in the hybrid scenario case: the normalized density gradient R/L_n, measured 1s after the start of the high power phase (and before the tungsten accumulates), varies between 2 and 3 when it is in the 1-1.5 range for 3.0-3.5MA baseline discharges in the same range of total injected power (20-26MW).

When the NBI and ICRH powers are applied, the density starts peaking 2-2.5s after the start of this high power phase and tungsten accumulates in the plasma core. The central temperature decreases but the normalized Te gradient is sometimes maintained high ($R/L_{Te}>4$). The resulting $R/L_n - 0.5R/L_{Te}$ parameter is positive (figure 17-a). No beneficial effect of the ICRH power between 3and 5MW on the core radiation ($r/a<0.3$) is observed but the total radiated power in the main plasma decreases strongly with the additional ICRH power: P_{rad}-Bulk/P_{tot} decreases from ~70% to 20% by just increasing the ICRH power by 2MW (figure 17-b). Tungsten and nickel radiations at mid-radius, derived from the NiXXIII line intensity, decrease identically to the total radiation. Although scans of IC resonance position have shown weak effect (and beneficial) of this parameter when the resonance is moved away on the LFS from the magnetic center on the tungsten radiation peaking (see section 3), there is still an uncertainty on the effect of very central ICRH ($r/a<0.1$) in the hybrid scenario.

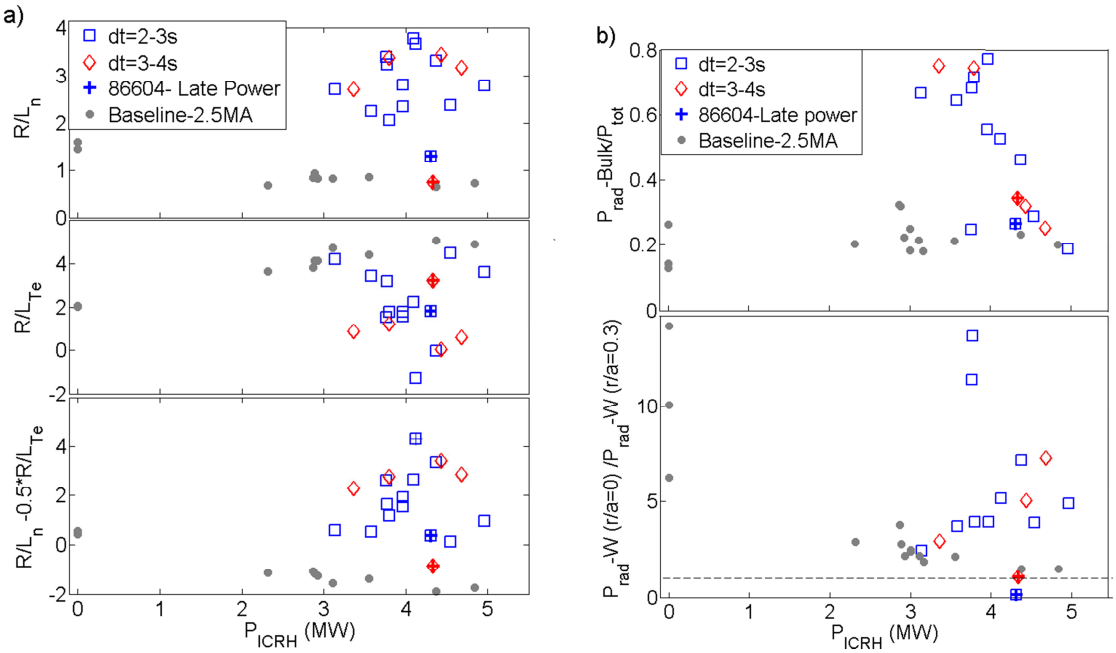

Figure 17) Normalized gradients b) P_{rad}-Bulk/P_{tot} and tungsten radiation peaking as a function of the ICRH power for two time slices after the start of the high power phase, dt=2-3s (squares), dt=3-4s (diamonds). B_t=2.9T, I_p=2.5MA, P_{tot}=22-27MW, F_{gas}=1.0-1.5×10^{22}el./s. Baseline discharges (2.7T/2.5MA) are indicated with close circles.

In one case, when the start of the high power phase was delayed by 0.5s (t_{start}=6s) and slightly more injected gas (1.3×10^{22}el./s), the low initial density peaking is maintained and even decreases during the high power phase (R/L_n decreases from 1.6 to 0.7). For this discharge, the tungsten radiation profile is maintained hollow with very low radiation in the core (<0.02MW/m^3 at r/a=0) for 3s. This discharge has chirping fishbones and a 1/1 mode with increasing amplitude. Similar discharge with earlier timing has a strong 3/2 mode. This NTM is a strong player in accelerating the impurity accumulation as previously observed [Hender 16]. However, the good confinement of the low tungsten core radiation discharge (H_{98y}~1.1, β_N~1.9) is not sustained beyond t- t_{start} =3s as the current profile evolves and the first sawtooth is triggered at t- t_{start}=2.5s.

6. Discussion and conclusions.

Modelling of Ion Cyclotron Resonance Heating in the hydrogen minority scheme indicates that both thermal deuterium and electrons are heated in JET plasmas with a ratio which does not depart from equipartition by very much after collisional redistribution in a wide range of hydrogen concentration. This is the result of the quite low RF power density on JET. ICRH

modelling also indicates that temperature screening from fast hydrogen ions could be roughly of the same magnitude than the one provided by the thermal deuterium ions, but the uncertainty is large due to the dependency on the derivative of the fast ion profile $dT_i/d\rho$. The screening is expected to be more effective at high hydrogen concentration, although the fast ion temperature decreases with n_H/n_e, but experiments do not show a beneficial effect of high hydrogen concentration on tungsten concentration in the plasma core. That could be the result of weaker absorption of the wave at high concentration.

Tungsten radiation in the plasma core, derived from the soft X-ray diagnostic, has been analyzed on a large data base covering the baseline scenario (I_p=2.5-4.0MA) and the hybrid scenario (I_p=2.5MA) with various gas injection rates.

For the baseline scenario, central ICRH is clearly efficient for reducing the tungsten accumulation in the plasma core. Peaking of the tungsten radiation is closely related to the peaking of the electron temperature peaking in the core (r/a~0.2) and is very likely related to the ion temperature peaking (see figure 4). The strongest electron heating (and less peaked tungsten profile) is provided by setting the IC resonance right at the center or slightly on the low field side and the minority concentration low (2-3%).

Using as a criteria for tungsten accumulation the ratio of W radiation at r/a=0 to r/a=0.3, spatially flux-surface averaged and temporally averaged on a sawtooth period at least 2.5 seconds after the start of the high power phase, flat or modestly peaked tungsten radiation (P_{rad}-W(r/a=0)/P_{rad}-W(r/a=0.3)<1.8) profiles are achieved with ~5MW of RF power either at low plasma current (I_p=2.5MA) or at higher plasma current (I_p=3MA) but with higher gas rate. For these H-mode discharges, the global confinement, which is the result of a complex combination of central high Z impurity content in the core and gas injection acting on the pedestal pressure but also beneficially on the tungsten source (by increasing the ELM frequency), is the highest ($H_{98,y}$~0.95) only for the 2.5MA discharges.

In the case of discharges carried out in the frame of the hybrid scenario, with P_{ICRH} in the 4-5MW range, strong tungsten accumulation occurs after ~2 seconds. This is correlated with the high initial peaking of the density inherent to this scenario. When this initial density peaking is slightly reduced, a very low tungsten concentration is observed and least peaked tungsten profile is provided for 3seconds after the start of the high power phase.

Beneficial effect of the fast ion population can be seen from the evolution of tungsten transport during a sawtooth cycle and the resulting fishbone activity grows in amplitude

when the tungsten radiation profile flattens (figure 11). Similarly, when the IC resonance position is moved, the tungsten peaking is minimized when the fishbone activity is maximized (figure 6). However, in the analyzed hybrid pulses for which neo-classical inward pinch is strong (resulting from peaked density profile) and/or the tungsten source is high, fishbones do not always prevent from tungsten accumulation.

The tungsten radiation peaking factor is consistent with the parameter R/L_n $-0.5R/L_{Te}$ which is used as a proxy for the neo-classical convection velocity which may drive impurity accumulation of heavy impurities, when the poloidal asymmetry arising from toroidal rotation is neglected The amplitude of this parameter is consistent with the W peaking factor for the various scenarios. In the baseline scenario, when ICRH is applied from the start of the high power phase, density peaking does not evolve by much when the ICRH power is increased from 3MW to 6MW and the improvement is caused by the increase of the R/T_e factor. In the hybrid scenario, the initial normalized density gradient R/L_{Te}, before the high power phase, is typically 2-3 times larger than in the baseline scenario case and ICRH power, up to 5MW, is not efficient to reverse the sign of the neo-classical transport parameter (R/L_n $-0.5R/L_{Te}$ >0). It is striking that by changing slightly the timing of the high power phase, increasing the gas rate by ~20% and the ICRH power by ~10%, the initial R/L_n is decreased by only ~10% and the density peaking further decreases steadily during the discharge to lower values than obtained for most of the pulses in the baseline scenario (R/L_n~0.7).

JET is preparing the D-T pulses which will be performed at higher power (P_{tot}>35MW). With the addition of the ILA antenna [Durodié 12] and further optimization of the ICRH system, 8-9MW could be achievable with a gas rate of ~1×10^{22}el./s. We can expect further improvement for controlling the tungsten concentration in the plasma core for the baseline scenario. The effect of ICRH for the hybrid scenario is more speculative, but sensitivity of the density peaking to the details of the scenario could be an opportunity for the effective control of tungsten accumulation while keeping good energy confinement for 5 seconds.

Acknowledgements

This work has been carried out within the framework of the EUROfusion Consortium and has received funding from the EURATOM research and training programme 2014-2018

under grant agreement No 633053. The views and opinions expressed herein do not necessarily reflect those of the European Commission.

References

[Angioni 2009] C.Angioni et al., Plasma Phys. Control. Fusion 51 (2009) 124017 (14pp) doi:10.1088/0741-3335/51/12/124017

[Angioni 2014] C.Angioni et al., Nucl. Fusion 54 (2014) 083028 (26pp) http://iopscience.iop.org/0741-3335/57/1/014031/pdf/0741-3335_57_1_014031.pdf

[Angioni 2015] C.Angioni et al., Physics of Plasmas 22, 055902 (2015) http://scitation.aip.org/content/aip/journal/pop/22/5/10.1063/1.4919036

[Beurskens 2014] M.N.A. Beurskens et al., Nucl. Fusion, 54 (2014) 043001, http://iopscience.iop.org/article/10.1088/0029-5515/54/4/043001/pdf

[Bilato 2014] R. Bilato, O. Maj and C. Angioni, Nucl. Fusion 54 (2014) 072003 (4pp) http://iopscience.iop.org/article/10.1088/0029-5515/54/7/072003/pdf

[Bobkov 2013] V. Bobkov et al., Journal of Nucl. Materials 438 (2013) S160–S165, http://www.sciencedirect.com/science/article/pii/S0022311513000524

[Breizman 2011] B N Breizman and S E Sharapov, Plasma Phys. Control. Fusion 53 (2011) 054001 (39pp) http://iopscience.iop.org/article/10.1088/0741-3335/53/5/054001/pdf

[Casson 2015] Casson F. Plasma Phys. Control. Fusion 57 (2015) 014031 (10pp) http://iopscience.iop.org/0741-3335/57/1/014031/pdf/0741-3335_57_1_014031.pdf

[Challis 2015] Challis C. et al., Nucl. Fusion 55 (2015) 053031 (18pp), http://iopscience.iop.org/article/10.1088/0029-5515/55/5/053031/pdf

[Colas 2006] L.Colas et al. Nucl. Fusion 46 (2006) S500–S513, http://iopscience.iop.org/0029-5515/46/7/S11

[Czarnecka 2014] A. Czarnecka et al., AIP Conf. Proc. 1580 (2014) p.227

[Den Harder 2016] N. Den Harder N. et al., Nucl. Fusion 56 (2016) 026014 (9pp) http://iopscience.iop.org/article/10.1088/0029-5515/56/2/026014/pdf

[Dumont 2009] Dumont R.J. 2009 Nucl. Fusion 49 075033 http://iopscience.iop.org/article/10.1088/0029-5515/49/7/075033/pdf

[Dumont 2013] R.J. Dumont and D. Zarzoso 2013 Nucl. Fusion 53 013002 http://iopscience.iop.org/article/10.1088/0029-5515/53/1/013002/pdf

[Durodié 12] F.Durodié et al., Plasma Phys. Control. Fusion 54 (2012) 074012 (16pp) http://iopscience.iop.org/article/10.1088/0741-3335/54/7/074012/pdf

[Giroud 2015] Giroud C. et al., Plasma Phys. Control. Fusion 57 (2015) 035004 (20pp) http://iopscience.iop.org/0741-3335/57/3/035004/pdf/0741-3335_57_3_035004.pdf

[Goniche 2014] Goniche M et al, Proc. 41st EPS Conf. Plasma Physics, Berlin, 23-27 June 2014, O4.129, http://ocs.ciemat.es/EPS2014ABS/pdf/O4.129.pdf

[Graves 2015] J.P.Graves et al., Plasma Phys. Control. Fusion **57** (2015) 014033 (14pp) http://iopscience.iop.org/article/10.1088/0741-3335/57/1/014033/pdf

[Hender 16] T.C.Hender et al, Nucl. Fusion 56 (2016) 066002 (15pp) http://iopscience.iop.org/article/10.1088/0029-5515/56/6/066002/meta

[Jacquet 13] P. Jacquet et al., Journal of Nuc. Materials 438 (2013) S379–S383 http://dx.doi.org/10.1016/j.jnucmat.2013.01.075

[Jacquet 14] P. Jacquet et al., Physics of Plasmas 21 (2014) pp.061510, http://scitation.aip.org/content/aip/journal/pop/21/6/10.1063/1.4884354

[Jacquet 16] P. Jacquet et al., Nucl. Fusion 56 (2016) 046001 (14pp)
http://iopscience.iop.org/article/10.1088/0029-5515/56/4/046001/pdf

[Kallenbach 05] Kallenbach A et al 2005 Plasma Phys. Control. Fusion, 47 B207 (2005) http://iopscience.iop.org/0741-3335/47/12B/S16

[Lerche 14] Lerche E. et al., Nucl. Fusion 56 (2016) 036022 (19pp)
http://iopscience.iop.org/article/10.1088/0029-5515/56/3/036022/pdf

[Lerche 14b] Lerche E. et al., Journal of Nucl. Materials 463 (2015) 634–639 http://www.sciencedirect.com/science/article/pii/S0022311514007582

[Klepper 13], C. Klepper et al., Journal of Nucl. Materials 438 (2013) S594–S598, http://www.sciencedirect.com/science/article/pii/S0022311513001323

[Lennholm 15] M. Lennholm et al., Nucl. Fusion **56** (2016) 016008
http://iopscience.iop.org/article/10.1088/0029-5515/56/1/016008/pdf

[Mantica 2014] P.Mantica, E.Puiatti, M.L.Reinke, M.Romanelli and JET EFDA contributors, Proc. 41th European Physical Society Conference on Plasma Physics, Berlin 2014, P1.107 (2014), http://ocs.ciemat.es/EPS2014PAP/pdf/P1.017.pdf.

[Mantica 2015] P. Mantica F.J.Casson, M.Valisa, C.Angioni, R.Bilato, E.Belonohy, C.Giroud, M.Goniche ,N.Hawkes, E. Lerche and JET contributors, Proc. 42th European Physical Society Conference on Plasma Physics, Lisbon 2015, P1.101 (2015), http://ocs.ciemat.es/EPS2015PAP/pdf/P1.101.pdf.

[Mantsinen 1999] Mantsinen M. et al , Plasma Phys. Control. Fusion 41 (1999) 843–865.
http://iopscience.iop.org/article/10.1088/0741-3335/41/7/301/pdf

[Mantsinen 2015] Mantsinen M. et al ; Proc. 42th European Physical Society Conference on Plasma Physics, Lisbon 2015, P2.171 (2015),

http://ocs.ciemat.es/EPS2015PAP/pdf/P2.171.pdf

[Nave 2003], M.F.F. Nave et al., Nucl. Fusion 43 (2003) 1204–1213 http://iopscience.iop.org/article/10.1088/0029-5515/43/10/023/pdf

[Nunes 2014], I.Nunes et al., Plasma Physics and Control. Fusion 58 (2016) 014034 (10 pp.) http://iopscience.iop.org/article/10.1088/0741-3335/58/1/014034/pdf

[Pütterich 2012] T. Pütterich, tungsten control in JET," in IAEA Fusion Energy Conference, San Diego, EX/P3–15 (2012), http://www-naweb.iaea.org/napc/physics/FEC/FEC2012/papers/193_EXP315.pdf.

[Pütterich 2013] T.Pütterich et al, Plasma Phys. Control. Fusion 55 (2013) 124036, http://iopscience.iop.org/0741-3335/55/12/124036/pdf/0741-3335_55_12_124036.pdf

[Valisa 2011] M.Valisa et al. ,Nucl. Fusion **51** (2011) 033002 (11pp) http://m.iopscience.iop.org/0029-5515/51/3/033002/pdf/0029-5515_51_3_033002.pdf

[Van Eester 14] D. Van Eester et al., EPS Confernce, Proc. 41st EPS Conf. Plasma Physics, Berlin, June 2014, http://ocs.ciemat.es/EPS2014ABS/pdf/P1.002.pdf